

# Quantum RNNs and LSTMs Through Entangling and Disentangling Power of Unitary Transformations

Ammar Daskin\*

Department of Computer Engineering,  
Istanbul Medeniyet University,  
Istanbul, Turkiye, 34000.

## Abstract

In this paper, we discuss how quantum recurrent neural networks (RNNs) and their enhanced version, long short-term memory (LSTM) networks, can be modeled using the core ideas presented in Ref. [1], where the entangling and disentangling power of unitary transformations is investigated. In particular, we interpret entangling and disentangling power as information retention and forgetting mechanisms in LSTMs. Therefore, entanglement becomes a key component of the optimization (training) process. We believe that, by leveraging prior knowledge of the entangling power of unitaries, the proposed quantum-classical framework can guide and help to design better-parameterized quantum circuits for various real-world applications.

**Keywords:** *quantum long short term memory, quantum LSTM, quantum RNN, entangling and disentangling parameterized circuits*

## 1 Introduction

For a unitary  $U$  that transforms an input state  $|\Psi_{\text{in}}\rangle$  to an output state  $|\Psi_{\text{out}}\rangle$  through  $|\Psi_{\text{out}}\rangle = U |\Psi_{\text{in}}\rangle$ , its entangling and disentangling powers, respectively,  $E^\uparrow(U)$  and  $E^\downarrow(U)$ , are defined as the maximum increase and decrease in entanglement between two subsystems after applying  $U$  [1]:

$$E^\uparrow(U) = \sup_{|\Psi_{\text{in}}\rangle} (E(\Psi_{\text{out}}) - E(\Psi_{\text{in}})), \quad (1)$$

$$E^\downarrow(U) = \sup_{|\Psi_{\text{in}}\rangle} (E(\Psi_{\text{in}}) - E(\Psi_{\text{out}})). \quad (2)$$

Linden et al.[1] have shown that for bipartite systems, although the entangling and disentangling power are the same for two-qubit unitaries, they differ in general

for unitaries of larger dimensions. As an example, they have demonstrated a qubit-qutrit unitary gate  $U_{2 \times 3}$  that can create 2 ebits of entanglement; however, the system cannot be fully disentangled using a similar unitary. Notably, for the inverse transformation  $U^\dagger$ , the relation  $E^\downarrow(U) = E^\uparrow(U^\dagger)$  holds since  $U^\dagger$  reverses the transformation effect of  $U$ .

This entangling power has been analytically investigated for bipartite permutation matrices [2] and two-qubit mixed states [3]. It has known upper bounds [4, 5] and can be maximized using perfect entangling gates [6, 7] or by incorporating ancilla qubits [1]. Additionally, it is relevant to communication capacity [8, 9] and has an influence over quantum circuit complexity [10].

The entangling and disentangling power of unitary transformations provide a framework for constructing a memory model in which entanglement can be explicitly quantified using previously analyzed unitaries. Consequently, a quantum machine learning model designed based on the entangling power of unitaries can be studied easier when we try to understand its expressivity and demonstrate its fundamental quantum advantages over classical counterparts.

The recurrent neural network (RNN) or long short-term memory (LSTM) cell models require a dynamic memory to retain or forget previous information. Previous works such as [11] or its quantum kernel-based version [12] use variational quantum circuits (VQCs) as subcomponents within a classical LSTM structure. The gates (forget, input, output) are replaced by VQCs, but the overall architecture remains mostly classical due to the use of classical memory. There are also several applications and comparison studies of these models with various variational circuit choices [13–18]. Ref. [19] discusses different design choices and provides implementation guidelines. Ref. [20] presents a fully quantum LSTM model, where the layers of a standard

\*adaskin25@gmail.com

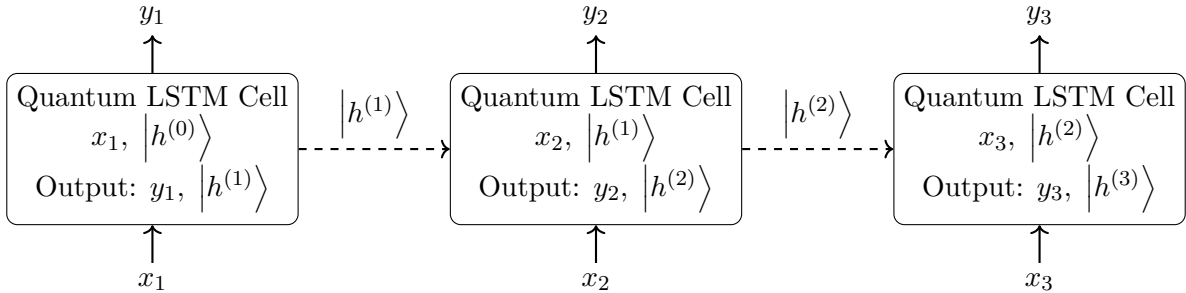


Figure 1: Generic Structure of Quantum LSTM.

LSTM are cascaded using ancilla registers and quantum multiplication and addition operations.

In this paper, we discuss how quantum RNNs and LSTMs can be modeled using the core ideas presented in Ref. [1], where the entangling and disentangling power can be directly related to information retention and forgetting, respectively. In particular, we consider the environment (ancilla) qubits as quantum memory representing the temporal hidden state of the model. Therefore, the quantum register acts as a memory, storing the history of the hidden state.

The optimization process in this model also involves optimizing how much entanglement is retained in the circuit. Although similar approaches can be observed in the previously discussed papers, we believe our work can pave the way for understanding how entanglement plays a role in carrying and propagating information in quantum machine learning models, especially LSTMs. Therefore, it can serve as a guide for determining a parameterized circuit choice in different applications, making entanglement a direct component of the learning process.

In the following sections, after explaining the general framework of the LSTM and its single LSTM cell in detail, we present numerical simulations on noisy random sine data to gauge the expressive power of the model. In addition, we present simulation results for weather data, demonstrating the model’s applicability to real-world scenarios.

## 2 The Hybrid General Framework

In a practical time-series task (such as forecasting), the model processes an ordered sequence of inputs:  $\{x_1, x_2, \dots, x_T\}$ , where each  $x_t$  is a scalar (or a feature vector) at time  $t$ . Our classical-quantum hybrid framework is based on using a quantum register for the input data  $x_t$  and an ancilla register for the hidden

state  $h_t$ .

One of the core principles in RNNs and LSTMs is the ability to sequentially process the given data, i.e., propagate information across time steps, which is referred to as hidden information. In our design, an ancilla register is used as a quantum memory to hold this hidden historical knowledge through its remaining entanglement with the system register from previous steps.

This general framework is depicted in Fig. 1. Each cell in this LSTM model represents an iteration, i.e., an application of a parameterized circuit to different inputs. The explicit details of an LSTM cell are given in Fig. 2. A high-level description for time step  $t$  can be enumerated as follows:

1. **Inputs:** The inputs to a cell are the classical data input  $x_t$  and the quantum hidden state  $|h^{(t-1)}\rangle$ , which propagates from the previous time step  $t-1$ .
  - (a) Since the classical input is a single value, it is projected onto a high-dimensional quantum state using an affine transformation [21, 22]. In particular, a classical scalar  $x_t \in \mathbb{R}$  is mapped by a linear layer to produce a vector  $\mathbf{a}_t = W_{x_t} x_t$ . This vector is then normalized to form a quantum state in the system subspace:

$$|\psi_x\rangle = \frac{1}{\|\mathbf{a}_t\|} \mathbf{a}_t \in \mathcal{H}_{\text{sys}}, \quad (3)$$

where  $\dim(\mathcal{H}_{\text{sys}}) = 2^{n_{\text{sys}}}$  represents the Hilbert space for the system register. Note that in our simulations, we have used  $n_{\text{sys}} = 2$ .

- (b) The hidden state is represented as a quantum state in the ancilla subspace and is typically initialized to a standard basis state. For example, we have used the following initial set-

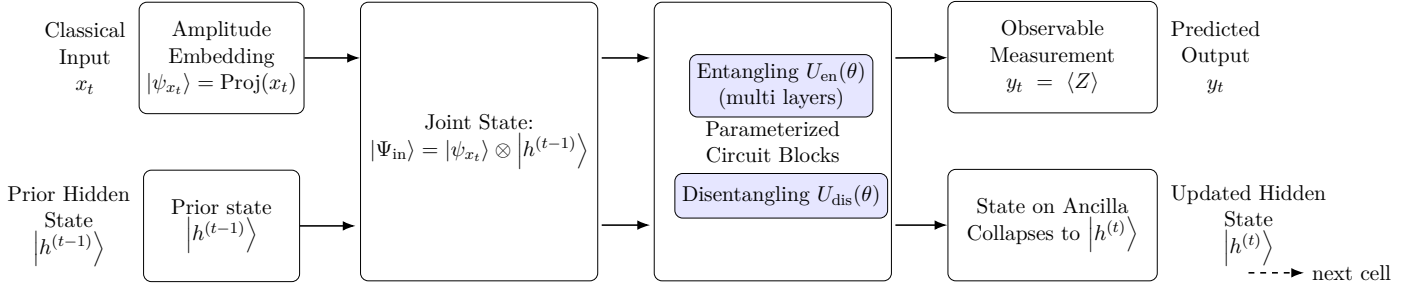


Figure 2: A Single Quantum LSTM Cell.

ting in our simulations:

$$|h^{(0)}\rangle = |0\rangle^{\otimes n_{\text{ancilla}}} = \begin{pmatrix} 1 \\ 0 \\ \vdots \\ 0 \end{pmatrix}. \quad (4)$$

2. **The input quantum state:** The whole joint state is given by:

$$|\Psi_{\text{in}}^{(t)}\rangle = |\psi_{x_t}\rangle \otimes |h^{(t-1)}\rangle \in \mathcal{H}_{\text{sys}} \otimes \mathcal{H}_{\text{ancilla}}. \quad (5)$$

Here,  $\mathcal{H}_{\text{ancilla}} = 2^{n_{\text{ancilla}}}$  represents the Hilbert space for the ancilla register, and in our simulations, we have used  $n_{\text{ancilla}} = 2$ . (In our simulations, the system and ancilla have the same sizes; however, this is not a requirement.) Note that this joint state is embedded into the quantum circuit via amplitude encoding.

3. **Parameterized Circuit:** We then apply two similarly structured quantum circuits,  $U_{\text{en}}$  and  $U_{\text{dis}}$ , with different parameters to emulate entangling and disentangling dynamics:

$$|\Psi_{\text{out}}^{(t)}\rangle = U_{\text{dis}} U_{\text{en}} |\Psi_{\text{in}}^{(t)}\rangle. \quad (6)$$

In the simulations, we have used a basic two-layer entangling circuit. One can increase the number of parameters in the model by choosing more complex designs. Note that, since the entangling and disentangling powers are different, we use similarly structured circuits with different trainable parameters in the hope that, by the end of the learning process, entanglement retention will be optimized.

4. **Final state and output extraction:** After the evolution by the parameterized circuit, the full state can be written in terms of its subspaces as:

$$|\Psi_{\text{out}}\rangle^{(t)} = \sum_{i=0}^{2^{n_{\text{sys}}}-1} |i\rangle_{\text{sys}} \otimes |\phi_i\rangle_{\text{ancilla}}, \quad (7)$$

where  $|i\rangle$  represents the  $i$ th basis in the standard basis, and each  $|\phi_i\rangle$  is an (unnormalized) state in the hidden (ancilla) Hilbert space. In quantum theory, after measurement, the quantum state becomes a mixed state that can be described by the reduced density matrix. In numerical simulations, one can obtain the reduced density matrix for the ancilla by tracing out the system qubits [23]:

$$\rho_{\text{ancilla}} = \text{Tr}_{\text{sys}} \left( |\Psi_{\text{out}}^{(t)}\rangle \langle \Psi_{\text{out}}^{(t)}| \right). \quad (8)$$

The state  $|\phi_i\rangle$  on the ancilla determines the probability  $p(i) = \|\phi_i\|^2$  associated with the system outcome  $|i\rangle_{\text{sys}}$  on the system register. Therefore, if we choose the  $i^*$  corresponding to the highest probability, then upon measurement of the system register, the state on the ancilla collapses to  $|\phi_{i^*}\rangle$ :

$$|\Psi_{\text{out}}^{(t)}\rangle \xrightarrow{\text{Measure}} |i^*\rangle_{\text{sys}} \otimes |h^{(t)}\rangle, \quad (9)$$

Thus, the hidden state is updated with the normalized ancilla component:

$$|h^{(t)}\rangle = \frac{|\phi_{i^*}\rangle}{\|\phi_{i^*}\|}. \quad (10)$$

Alternatively, in the simulations, we have also employed the normalized diagonal of the density matrix:

$$|h^{(t)}\rangle = \text{diag}(\rho_{\text{ancilla}}). \quad (11)$$

While  $|\phi_{i^*}\rangle$  is composed of amplitudes, this vector contains the probabilities  $[p_0, p_1, \dots, p_{2^{n_{\text{ancilla}}}-1}]$ , where  $p_j = \langle j | \rho_{\text{ancilla}} | j \rangle$ . On a quantum machine, when the size of the ancilla register is small (as in our simulations, where it consists of only a few qubits), one can approximate the full tomography of the state by using a few repetitions of the circuit. However, for larger ancilla sizes, a more computationally efficient choice would be to measure

individual qubits and combine their results to obtain an approximate representation of the previous hidden state.

Note that transitioning from amplitudes to probabilities and then to individual probabilities (or one-zero outcomes) inherently leads to information loss. The appropriate choice can be determined based on the application, as some applications may be resilient to such losses (e.g., data points that are less likely to depend on previously observed values).

Alongside updating the hidden state, the circuit also computes an expectation value of an observable on one of the system qubits. The chosen qubit (or qubits if  $y_t$  is a vector) can be selected from among the system qubits. Then, the predicted output is:

$$y_t = \langle \Psi_{\text{out}}^{(t)} | Z_m | \Psi_{\text{out}}^{(t)} \rangle, \quad (12)$$

where  $Z_m$  denotes a measurement operator, e.g., the Pauli-Z operator on a chosen qubit.

5. **Optimization (training):** The sequence of outputs  $\{y_t\}$  is collected to form the output of the cell for that input sequence. A classical loss function (we use mean squared error (MSE) in numerical simulations) is computed between the predicted outputs and the target values. The network is trained end-to-end via backpropagation, even though the collapse operation simulating an actual projective measurement is non-differentiable. However, it can be estimated using the parameter-shift rule [22].

As explained in the above steps and as also shown in Fig. 1, propagating information to the next cell is done through a collapsed quantum state or by obtaining a partial tomography. Collapsing a quantum state is achieved by measuring the system register, which can involve sequentially aligned individual qubit measurements or a full quantum register measurement. Therefore, it is important to point out that the required number of qubits is directly related to the circuit output (which, for time-series tasks, is generally a scalar) and the number of parameters used to train the model. If the quantum architecture allows such mid-level quantum circuit measurements, then this model can be implemented directly on such an architecture, as it would require only a limited number of qubits.

### 3 Numerical Simulations

Here, note that the simulation code can be fully downloaded, and the results can be regenerated using the link provided in the data availability section. In the code, the flowchart given in Fig. 3 is implemented in two different ways: separately for the reduced density matrix formalism and the collapsed state formalism.

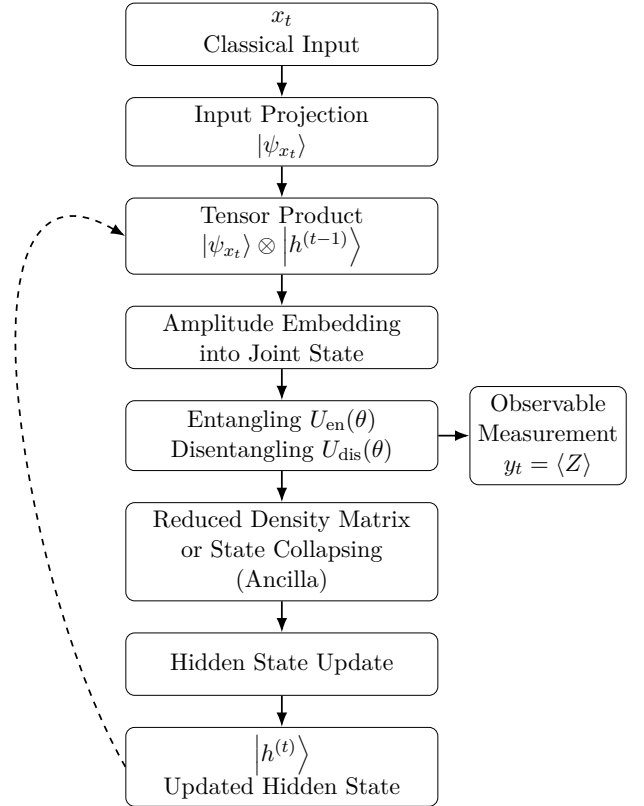


Figure 3: Numerical Steps Used to Simulate Quantum LSTM.

The simulation code uses the PennyLane [21] Python library for generating quantum circuits and its machine learning libraries, along with PyTorch for training the model. For the entangling and disentangling gates, we have used the PennyLane quantum library to generate a basic entangling gate, with a similar structure used for the disentangling gate. Both of these operators use separate trainable parameters.

To study the expressive power of the model, we have used a noisy sine function. To demonstrate its applicability to real-world problems, we have used one year of weather data from Ontario, Canada.

- The noisy sine data is generated by first creating 100 values in the range  $[0, 8\pi]$ , computing their

sine, and then adding different random noise between  $[-0.1, 0.1]$  to each function value. As in classical training schemes, the data is divided into two partitions: 80% for training and 20% for testing. We choose 5 for the batch size and 0.01 for the learning rate. After random sampling, 80% of the data is used for training, and the remaining 20% is used for testing. For both the reduced density matrix and the collapsed state computations, Fig. 4 shows the loss values during training, as well as the predicted and true values for the test portion of the data (the 20% separated part).

- We have also taken 365 days of weather data between 10 May 2024 and 10 May 2025 for Ontario, Canada [24, 25]. With settings similar to those used for the sine function, we run the simulations. The results are reported in Fig. 5.

As seen from both figures, the model is mostly able to predict the expected values. We can also see that when we use the collapsed state, the loss exhibits small sharp upward jumps. This may be a good indication that the model has the ability to jump over local minima when it gets stuck. As mentioned before, for more complex datasets, accuracy can be improved by using more layered parameterized circuits or increasing the number of qubits, both of which enhance the expressive power of quantum machine learning models but make training more difficult [26, 27].

## 4 Conclusion

In this paper, we have described a quantum LSTM model in which the entanglement between the system and environment directly encodes memory by mimicking the entangling and disentangling power difference of unitary transformations. In previous models, entanglement is not used to store memory; rather, it primarily aids in feature extraction while enhancing the ability of a parameterized circuit to model nonlinearities (e.g., via CNOT gates). In our model, however, entanglement is explicitly considered as part of the optimization process. Therefore, our model can leverage prior knowledge of the entangling power of unitary transformations to design application-specific parameterized circuits and machine learning models.

## 5 Data availability

The simulation code used to generate all figures presented in this paper is publicly available on: <https://github.com/adaskin/quantum-lstm>

[//github.com/adaskin/quantum-lstm](https://github.com/adaskin/quantum-lstm)

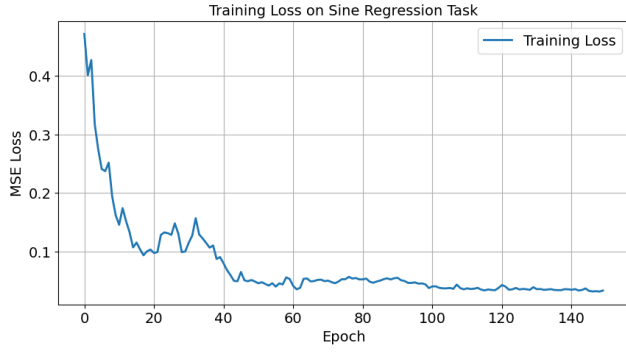
## 6 Funding

This project is not funded by any funding agency.

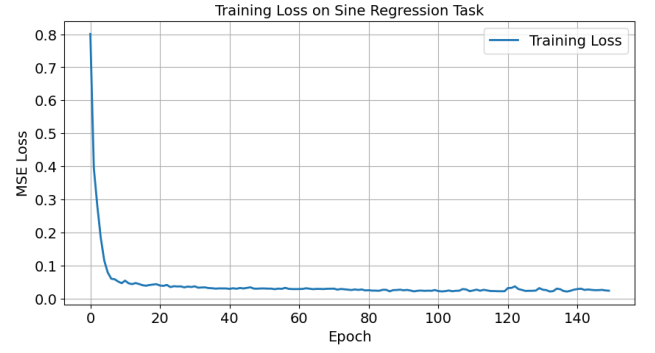
## References

- [1] Noah Linden, John A Smolin, and Andreas Winter. Entangling and disentangling power of unitary transformations are not equal. *Physical review letters*, 103(3):030501, 2009.
- [2] Lin Chen and Li Yu. Entangling and assisted entangling power of bipartite unitary operations. *Physical Review A*, 94(2):022307, 2016.
- [3] Zhe Guan, Huan He, Yong-Jian Han, Chuan-Feng Li, Fernando Galve, and Guang-Can Guo. Entangling power of two-qubit gates on mixed states. *Physical Review A*, 89(1):012324, 2014.
- [4] Sergey Bravyi. Upper bounds on entangling rates of bipartite hamiltonians. *Physical Review A—Atomic, Molecular, and Optical Physics*, 76(5):052319, 2007.
- [5] Siddhartha Das, Stefan Bäuml, and Mark M Wilde. Entanglement and secret-key-agreement capacities of bipartite quantum interactions and read-only memory devices. *Physical Review A*, 101(1):012344, 2020.
- [6] Marcin Musz, Marek Kuś, and Karol Życzkowski. Unitary quantum gates, perfect entanglers, and unistochastic maps. *Physical Review A—Atomic, Molecular, and Optical Physics*, 87(2):022111, 2013.
- [7] Nengkun Yu, Runyao Duan, and Mingsheng Ying. Optimal simulation of a perfect entangler. *Physical Review A—Atomic, Molecular, and Optical Physics*, 81(3):032328, 2010.
- [8] Aram W Harrow and Peter W Shor. Time reversal and exchange symmetries of unitary gate capacities. *arXiv preprint quant-ph/0511219*, 2005.
- [9] Stefan Bäuml, Siddhartha Das, and Mark M Wilde. Fundamental limits on the capacities of bipartite quantum interactions. *Physical Review Letters*, 121(25):250504, 2018.

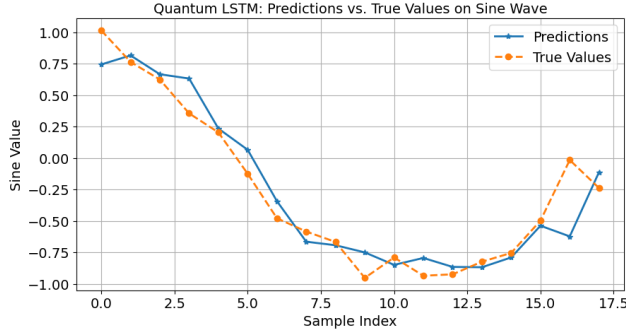
- [10] Jens Eisert. Entangling power and quantum circuit complexity. *Physical Review Letters*, 127(2): 020501, 2021.
- [11] Samuel Yen-Chi Chen, Shinjae Yoo, and Yao-Lung L Fang. Quantum long short-term memory. In *Icassp 2022-2022 IEEE international conference on acoustics, speech and signal processing (ICASSP)*, pages 8622–8626. IEEE, 2022.
- [12] Yu-Chao Hsu, Tai-Yu Li, and Kuan-Cheng Chen. Quantum kernel-based long short-term memory. *arXiv preprint arXiv:2411.13225*, 2024.
- [13] Saad Zafar Khan, Nazeefa Muzammil, Salman Ghafoor, Haibat Khan, Syed Mohammad Hasan Zaidi, Abdulah Jeza Aljohani, and Imran Aziz. Quantum long short-term memory (qlstm) vs. classical lstm in time series forecasting: a comparative study in solar power forecasting. *Frontiers in Physics*, 12:1439180, 2024.
- [14] Aditi Saha, Taieba Tasnim, Mohammad Rahman, and Fan Wu. Advancing time series forecasting: Quantum vs. classical lstm approaches. In *2025 IEEE 15th Annual Computing and Communication Workshop and Conference (CCWC)*, pages 00196–00202. IEEE, 2025.
- [15] Prashanth Choppara and Bommareddy Lokesh. Leveraging quantum lstm for high-accuracy prediction of viral mutations. *IEEE Access*, 2025.
- [16] Sarvapriya Tripathi, Himanshu Upadhyay, and Jayesh Soni. A quantum lstm-based approach to cyber threat detection in virtual environment. *The Journal of Supercomputing*, 81(1):142, 2025.
- [17] Tariq Mahmood, Ibtasam Ahmad, Malik Muhammad Zeeshan Ansar, Jumanah Ahmed Darwish, and Rehan Ahmad Khan Sherwani. Comparative study of long short-term memory (lstm) and quantum long short-term memory (qlstm): Prediction of stock market movement. *arXiv preprint arXiv:2409.08297*, 2024.
- [18] Anupama Padha and Anita Sahoo. Qclr: Quantum-lstm contrastive learning framework for continuous mental health monitoring. *Expert Systems with Applications*, 238:121921, 2024.
- [19] Yifan Zhou, Chong Cheng Xu, Mingi Song, Yew Kee Wong, and Kangsong Du. Implementation guidelines and innovations in quantum lstm networks. *arXiv preprint arXiv:2406.08982*, 2024.
- [20] Andrea Ceschini, Antonello Rosato, and Massimo Panella. Design of an lstm cell on a quantum hardware. *IEEE Transactions on Circuits and Systems II: Express Briefs*, 69(3):1822–1826, 2021.
- [21] Ville Bergholm, Josh Izaac, Maria Schuld, Christian Gogolin, Shah Nawaz Ahmed, Vishnu Ajith, M Sohaib Alam, Guillermo Alonso-Linaje, B Akash Narayanan, Ali Asadi, et al. PennyLane: Automatic differentiation of hybrid quantum-classical computations. *arXiv preprint arXiv:1811.04968*, 2018.
- [22] Maria Schuld and Francesco Petruccione. *Machine learning with quantum computers*, volume 676. Springer, 2021.
- [23] Michael A Nielsen and Isaac L Chuang. *Quantum computation and quantum information*. Cambridge university press, 2010.
- [24] Meteostat. Meteostat - open weather & climate data, 2025. URL <https://meteostat.net>. Accessed: 2025-05-11.
- [25] Christian Sebastian Lamprecht. Meteostat python, 2025. URL <https://orcid.org/0000-0003-3301-2852>.
- [26] Jarrod R McClean, Sergio Boixo, Vadim N Smelyanskiy, Ryan Babbush, and Hartmut Neven. Barren plateaus in quantum neural network training landscapes. *Nature communications*, 9(1): 4812, 2018.
- [27] Martín Larocca, Supanut Thanasilp, Samson Wang, Kunal Sharma, Jacob Biamonte, Patrick J Coles, Lukasz Cincio, Jarrod R McClean, Zoë Holmes, and M Cerezo. Barren plateaus in variational quantum computing. *Nature Reviews Physics*, pages 1–16, 2025.



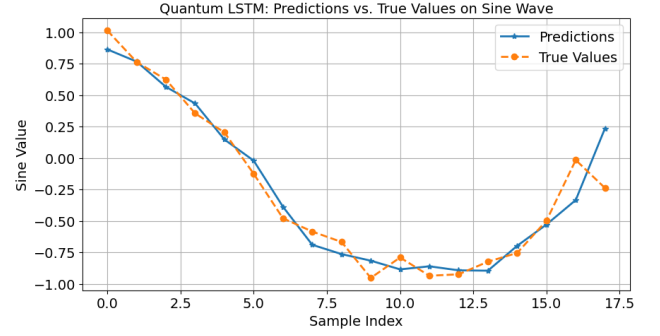
(a) Loss when collapsed state is used for hidden state



(b) Loss when probabilities are used for hidden state

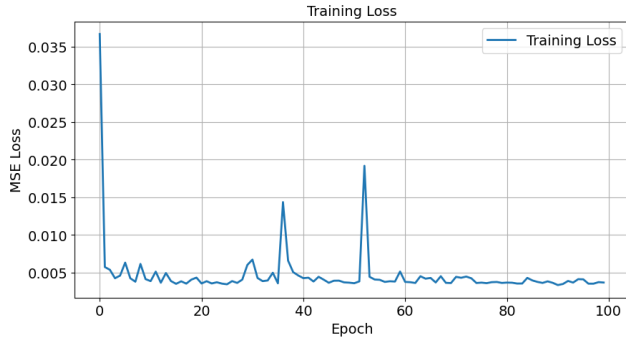


(c) Predictions vs true values for the test cases when collapsed state is used for hidden state

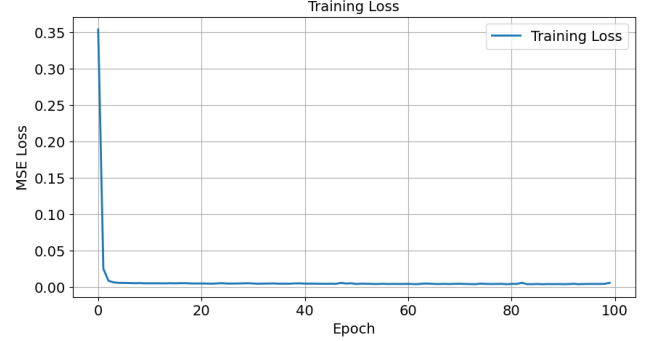


(d) Predictions vs true values for the test cases when probabilities are used for hidden state

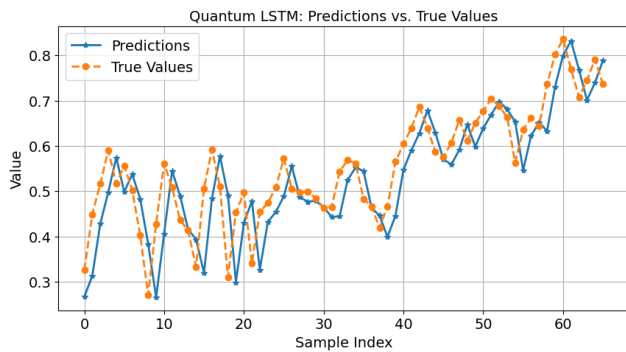
Figure 4: The loss and the predictions vs true values in the test cases of the noisy sine function for the values in range  $[0, 8\pi]$ .



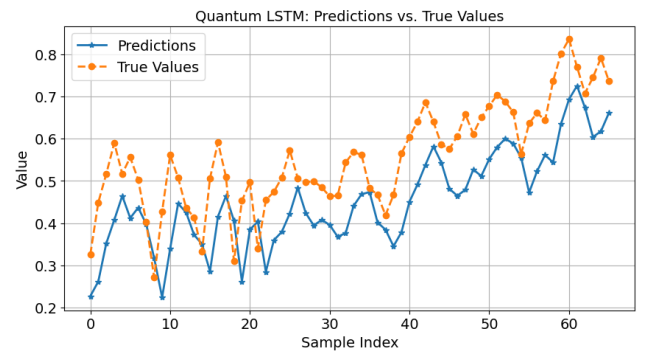
(a) Loss when collapsed state is used for hidden state



(b) Loss when probabilities are used for hidden state



(c) Predictions vs true values for the test cases when collapsed state is used for hidden state



(d) Predictions vs true values for the test cases when probabilities are used for hidden state

Figure 5: The loss and the predictions vs true values in the test cases of the weather data for Ontario, Canada.